

DR. ANPING CHEN (Orcid ID : 0000-0003-2085-3863)

DR. DANIEL RICCIUTO (Orcid ID : 0000-0002-3668-3021)

DR. JINGFENG XIAO (Orcid ID : 0000-0002-0622-6903)

Article type : Primary Research Article

Seasonal changes in GPP/SIF ratios and their climatic determinants across the Northern Hemisphere

Anping Chen^{1,*}, Jiafu Mao^{2,*}, Daniel Ricciuto², Dan Lu², Jingfeng Xiao³, Xing Li³, Peter E. Thornton², Alan K. Knapp¹

¹ Department of Biology and Graduate Degree Program in Ecology, Colorado State University, Fort Collins, CO, USA

² Environmental Sciences Division and Climate Change Science Institute, Oak Ridge National Laboratory, Oak Ridge, TN, USA

³ Earth Systems Research Center, Institute for the Study of Earth, Oceans, and Space, University of New Hampshire, Durham, NH, USA

This article has been accepted for publication and undergone full peer review but has not been through the copyediting, typesetting, pagination and proofreading process, which may lead to differences between this version and the [Version of Record](#). Please cite this article as [doi: 10.1111/gcb.15775](https://doi.org/10.1111/gcb.15775)

This article is protected by copyright. All rights reserved

Accepted Article

* Correspondence should be sent to anping.chen@colostate.edu (A.C.) and maoj@ornl.gov (J. M.)

Abstract

Satellite derived sun-induced chlorophyll fluorescence (SIF) has been increasingly used for estimating gross primary production (GPP). However, the relationship between SIF and GPP has not been well defined, impeding the translation of satellite observed SIF to GPP. Previous studies have generally assumed a linear relationship between SIF and GPP at daily and longer time scales, but support for this assumption is lacking. Here we used the GPP/SIF ratio to investigate seasonal variations in the relationship between SIF and GPP over the Northern Hemisphere (NH). Based on multiple SIF products and MODIS and FLUXCOM GPP data, we found strong seasonal hump-shaped patterns for the GPP/SIF ratio over northern latitudes, with higher values in the summer than in the spring or autumn. This hump-shaped GPP/SIF seasonal variation was confirmed by examining different SIF products and was evident for most vegetation types except evergreen broadleaf forests. The seasonal amplitude of the GPP/SIF ratio decreased from the boreal/arctic region to drylands and the tropics. For most of the NH, the lowest GPP/SIF values occurred in October or September, while the maximum GPP/SIF values were evident in June and July. The most pronounced seasonal amplitude of GPP/SIF occurred in intermediate temperature and precipitation ranges. GPP/SIF was positively related to temperature in the early and late parts of the growing season, but not during the peak growing months. These shifting relationships between temperature and GPP/SIF across different months appeared to play a key role in the seasonal dynamics of GPP/SIF. Several mechanisms may explain the patterns we observed and future research encompassing a broad range of climate and vegetation settings is needed to improve our understanding of the spatial and temporal relationships between SIF and GPP. Nonetheless, the strong seasonal variation in GPP/SIF we identified highlights the importance of incorporating this behavior into SIF-based GPP estimations.

Keywords: sun-induced chlorophyll fluorescence (SIF), gross primary production (GPP), GPP/SIF ratio, seasonal variation, seasonal amplitude, climate determinant

Introduction

Accurate quantifying the dynamics of plant photosynthetic carbon inputs into ecosystems (e.g., gross primary production; GPP), at broad geographical scales is fundamental to understanding how global changes are influencing the Earth system (Beer et al., 2010; Sitch et al., 2008; Turner et al., 2003; Xiao et al., 2010). Since the 1980s, remote sensing has increasingly been used for regional and global-scale GPP estimation (Hilker et al., 2008; Prince and Goward, 1995; Tucker et al., 1986), and numerous remote sensing-based GPP products are widely used in ecological, environmental, and Earth science research (Running et al., 2004; Yuan et al., 2010). Despite these advances, there is still considerable uncertainty in the quantification of regional and global GPP and thus carbon cycling (Anav et al., 2015; Keenan et al., 2012; Sjöström et al., 2013). The difficulty arises, in part, because most remote sensing-based GPP products are derived from light use efficiency models and these often represent GPP potential but not actual photosynthetic amount (He et al., 2013; Turner et al., 2006). The recent emergence of sun-induced chlorophyll fluorescence (SIF) data from satellite-based instruments can help resolve this uncertainty by providing observations that are more strongly related to actual photosynthetic carbon uptake (Frankenberg et al., 2011; Guanter et al., 2014; Mohammed et al., 2019; Parazoo et al., 2014; Sun et al., 2017). Specifically, satellite SIF retrieves the fluorescence signal that is emitted from canopy-scale photosynthetic activity (Joiner et al., 2011; Meroni et al., 2009). However, if SIF is to provide accurate GPP estimates, the relationship between SIF and GPP needs to be understood and quantified (Porcar-Castell et al., 2014).

It is commonly accepted that GPP increases linearly with SIF (Guanter et al., 2012; Li et al., 2018; Sun et al., 2017; Yang et al., 2017; Zhang et al., 2016). However, whether this linear relationship is constant or varies across different regions and vegetation types remains uncertain (Gu et al., 2019; Xiao et al., 2019; Zhang et al., 2018). Using the ratio of GPP/SIF as a metric of the SIF-GPP relationship, we showed previously that this relationship can vary substantially at large spatial scales and depending on climate, with water availability as the primary factor governing geographic variation in growing season GPP/SIF ratios (Chen et al., 2020). We found that GPP/SIF ratios increased from dry-and-hot to wet-and-cold climates, which may be related to moisture regulated stomatal responses and leaf shape and clustering patterns (Chen et al., 2020). While more definitive determinants of the primary mechanisms underlying spatial variation in SIF-GPP relationships are

needed, it is clear that the use of SIF for GPP monitoring and the use of SIF-derived GPP to constrain carbon cycle model predictions require understanding how both location and climate affect this relationship.

While progress has been made in assessing spatial variation in the SIF-GPP relationship, defining and better understanding the temporal dynamics of this relationship is also needed.

Evaluating how the SIF-GPP relationship changes within the growing season for a given location is necessary to more accurately predict GPP from SIF data. Importantly, because vegetation type can usually be safely assumed to be constant within a year, knowledge of the potential variation in seasonal GPP/SIF ratios may provide additional insight needed for understanding mechanisms governing the variation of SIF-GPP relationship in both space and time (Jeong *et al.*, 2017; Magney *et al.*, 2019; Porcar-Castell *et al.*, 2014).

Here, using multiple SIF datasets, we investigated how the SIF-GPP relationship varies across the growing season cycle in the Northern Hemisphere (NH). The aim of this study is to improve our understanding on the SIF-GPP relationship and its controlling factors from a seasonal cycle perspective. We hypothesized, based on our earlier analyses (Chen *et al.*, 2020), that the seasonal course of GPP/SIF ratios would be unimodal or hump-shaped driven by climatic seasonality (H1), with higher values in the summer than in spring or autumn. Because climatic seasonality shows a clear latitudinal pattern, we also hypothesized that potential seasonality of GPP/SIF would be strongest in the boreal and arctic regions, intermediate in the temperate, and least dynamic in the tropics (H2). Furthermore, as climatic variables such as temperature and precipitation and their roles as limiting factors for plant photosynthesis vary considerably across different seasons (e.g., Tan *et al.*, 2015), we thus further hypothesized that correlations between climatic factors and GPP/SIF would change across different seasons, consistent with seasonal pattern of GPP/SIF variations (H3).

2. Data and Methods

As we focused primarily on seasonal variation of the relationship between SIF and GPP, we used the GPP/SIF ratio as a diagnostic metric for this relationship. To assess the robustness of the GPP/SIF ratio and its temporal variations, we used four sets of gridded and contiguous SIF data from

different satellite sensors, which are the Global Ozone Monitoring Experiment-2 (GOME-2; Joiner *et al.*, 2013), Greenhouse Gases Observing Satellite (GOSAT; Frankenberg *et al.*, 2011), Orbiting Carbon Observatory 2 (OCO-2; Sun *et al.*, 2017), and Tropospheric Monitoring Instrument (TROPOMI; Köhler *et al.*, 2018). Note the coverage of the native SIF data from the OCO-2 sensor are spatially discontinuous, and some methods are needed to gap-fill the observations to derive a fully covered SIF product. Here we used the one developed by Li & Xiao (2019; GOSIF) which is a dataset derived from OCO-2 SIF soundings using a machine learning method. While these SIF products have different spatial and temporal resolutions and coverages, we linearly interpolated all the datasets to a common 1° by 1° spatial resolution. All SIF datasets have been daily corrected for comparability (Frankenberg *et al.*, 2011; Zhang *et al.*, 2018). Details about these SIF datasets and their processing can be found in Chen *et al.* (2020). In particular, we normalized each GPP and SIF product within the range of [0,1] by min-max scaling. It should be noted that this normalization does not change the results, as evidenced by analyses with un-normalized original data we will present in supplementary figures. When using un-normalized data, we excluded grids/months with SIF values $< 0.1 \text{ mW m}^{-2} \text{ sr}^{-1} \text{ nm}^{-1}$, since a very small value in the division would generate exceptionally large GPP/SIF values and cause spurious seasonal variations (Fig. S1).

We used data-driven modelled GPP products from both FLUXCOM (ftp://ftp.bgc-jena.mpg.de/pub/outgoing/FluxCom/CarbonFluxes/RS_METEO/member/) and MOD17A2 GPP (MODIS GPP; Zhao and Running, 2010). Monthly FLUXCOM GPP, currently available for 1982–2018, was upscaled from eddy covariance tower measurements using multiple machine learning algorithms trained with meteorological measurements and satellite data (Tramontana *et al.*, 2016), each generating a set of GPP product. Here we used the average of these GPP products. MODIS GPP from 2000–2018 was obtained from NASA's Land Processes Distributed Active Archive Center (LP DAAC) and was calculated using a light use efficiency model forced by satellite observations and climate data (Zhao and Running, 2010). The original spatial resolution of FLUXCOM GPP is 0.5° by 0.5° , and that of MODIS GPP is 0.05° by 0.05° spatial resolution. We aggregated both datasets to 1° by 1° to match that of SIF products, and calculated the mean value of FLUXCOM GPP and MODIS GPP. As we will show in supplementary result figures, the use of the mean value from the two GPP products does not affect the robustness of the results. Because growing season length clearly changes

across the NH, we used grid-specific growing season length following Zhu *et al.* (2016). For each month during the location-specific growing season, we calculated multi-year mean GPP/SIF ratio for each SIF product.

We also used dominant land cover class from the Moderate-Resolution Imaging Spectroradiometer (MODIS) MCD12C1 C5.1 product (Friedl *et al.*, 2010), for 2010 and at a spatial resolution of 0.05°. This data adopts the International Geosphere-Biosphere Programme (IGBP) land cover classification scheme (Loveland and Belward, 1997), consisting of 17 major land cover classes. The ‘closed shrublands’ and ‘open shrublands’ classes were combined as ‘shrublands’, and the ‘woody savannas’ was grouped into the ‘savannas’ class. In this study, we used 10 major vegetation types, or plant functional types (PFTs), including evergreen needle-leaf forest (ENF), evergreen broad-leaf forest (EBF), deciduous needleleaf forest (DNF), deciduous broadleaf forest (DBF), mixed forest (MF), shrublands (SHR), savannas (SAV), grasslands (GRA), permanent wetlands (WET), croplands (CRO). To match with the SIF data, land cover data were aggregated to 1° by 1° grids by selecting the class in each grid that occurs most often.

The global land was also divided into four climate zones based on the Köppen–Geiger classification system (Peel *et al.*, 2007): tropics, dryland, temperate, and boreal/arctic. Specifically, the tropics is the Köppen-Geiger A (tropical) climate group; the dryland is the Köppen-Geiger B (dry) climate group; the temperate region is the Köppen-Geiger C (mild temperate) climate group; and the boreal region is defined as the Köppen-Geiger D (continental) and E (polar) climate groups.

We used climate (temperature (TMP) and precipitation (PRE)) data from the Climatic Research Unit (CRU) (Harris *et al.*, 2014) v4.0.1 data set (<http://www.cru.uea.ac.uk/data/>) aggregated to 1° by 1° grids. This dataset is originally at the 0.5° by 0.5° spatial resolution. We also used downward shortwave radiation (SWR) data provided by the CRUNCEP V8 reanalysis (Viovy, 2016).

To understand potential climatic control on GPP/SIF and its seasonal variation, we performed partial correlations between GPP/SIF and climatic and radiation factors (TMP, PRE, and SWR) for each month. Such partial correlation analyses were conducted for different regions and vegetation types, as well as for each 1° by 1° grid cell. For grid-level partial correlation analysis, we used 9° by 9° degree moving windows centered at each grid cell. We also conducted a random forest modelling

analysis to identify dominant drivers for the spatial variations of GPP/SIF. Given that climatic conditions of previous months may affect vegetation productivity (Buermann *et al.*, 2018; Fu *et al.*, 2014; 2015) and thus the GPP/SIF ratio, we included climatic factors of both the focused month and its “pre-season” months in the random forest model. Here, pre-season is defined as consecutive (no more than three) months immediately preceding the focused month when the climatic factor shows the strongest spatial correlation with GPP/SIF of the focused month.

3. Results

We found a clear unimodal “hump-shaped” seasonal pattern of GPP/SIF over the Northern Hemisphere (Fig. 1), confirming H1. As a comparison, the seasonal patterns of both GPP and SIF were also hump-shaped (Fig. S2). Regionally, this hump-shaped GPP/SIF seasonality was strongest for the boreal/arctic region, followed by the temperate region. Moving south, the seasonality diminished in drylands, and in the tropics the monthly GPP/SIF curve becomes flat (Fig. 1). This decreasing seasonality of GPP/SIF from the higher to lower latitudes also confirms our hypothesis H2. Importantly, the hump-shaped pattern of GPP/SIF over the entire Northern Hemisphere, as well as the decrease of this hump shape from the boreal/arctic region to temperate and then to tropics and drylands, was consistent across all four satellite SIF products, as well as when using FLUXCOM and MODIS GPP products separately (Fig. 1, Fig. S3). In addition, this unimodal “hump-shaped” seasonal pattern of GPP/SIF was again revealed when calculating with the original GPP and SIF values without normalization (Fig. S4).

This hump-shaped GPP/SIF change across the growing season was also observed for most vegetation types. As shown in Fig. 2, except for the evergreen broadleaf forests (EBF) that dominate the tropics, all the other vegetation types are characterized with the hump-shaped GPP/SIF curve consistently across all the four SIF products, including evergreen needle forest (ENF). This latter vegetation type is notable because here seasonal variations in leaf area is minimal (Xu *et al.*, 2016). Except for EBF, the amplitude of seasonal variation (ASV) of GPP/SIF, defined as the difference between the maximum and minimum monthly GPP/SIF values within the growing season, was greater for forests than for other vegetation types including cropland (CRO), grassland (GRA), savannah

(SAV), and shrubland (SHR), which was also consistent across all the SIF products (Fig. 2). Wetland vegetation (WET) was observed with hump-shaped seasonal GPP/SIF patterns for SIF derived by GOME-2, GOSIF, and TROPOMI, but not for that by GOSAT (Fig. 2). GPP/SIF of WET was also much higher than that of other vegetation types by GOSIF.

Across the space, ASV was highest in the boreal forest region, decreasing toward temperate and then drylands and tropics. This spatial pattern again confirms our earlier finding of the regional pattern in GPP/SIF seasonality (Fig. 1). The pattern was also consistently found by all the SIF products; the only obvious difference among these products was the much smaller ASV by GOME-2 SIF than for other SIF products in the boreal forest area (Fig. 3).

As results based on different SIF products consistently revealed highly similar patterns and findings, hereafter we only used results derived from GOME-2 SIF for demonstration, unless otherwise noted. Fig. 4 shows the spatial distribution of the months with the minimum and maximum GPP/SIF values. For most of the Northern Hemisphere, October or September was the month with the lowest GPP/SIF values (Fig. 4a). The distribution of the month of the maximum GPP/SIF values was also heterogeneous, with July and June being the most common ones (Fig. 4b). For most of eastern China, August was the month with the highest GPP/SIF values. In India, the highest GPP/SIF values often occurred in September. For sub-Saharan Africa, the highest values were generally found in August, September, or October (Fig. 4b). Furthermore, similar patterns were found by examining individual SIF products (Fig. S5).

As potential non-linearity of the GPP-SIF relationship or the intercept of a linear GPP-SIF relationship may change GPP/SIF ratios, we also compared the GPP-SIF relationship across growing-season months (Mar-Oct) built with a linear and a non-linear (quadratic) model. We found that over boreal and temperate areas, the linear model shows similar performance as non-linear models in characterizing the GPP-SIF relationship. However, over some tropical regions, dry and arctic regions, the quadratic model can better fit cross-month GPP-SIF relationships than the linear model (Fig. S6).

We also examined how the observed variation of GPP/SIF across different months during the growing season may be related to climatic variations. Over the entire Northern Hemisphere, temperature was positively related to GPP/SIF during the early and late season; yet this positive

partial correlation between GPP/SIF and temperature turned to be close to zero for peak growing months (Fig. 5a). This hump shaped importance of temperature control of GPP/SIF variations was also found in temperate, dryland, and boreal/arctic regions (Fig. 5a). However, for both drylands and temperate regions, the partial correlation coefficient between temperature and GPP/SIF was negative during the peak growth months. In boreal/arctic regions, the partial correlation between temperature and GPP/SIF was significantly positive across all months and less variant, with the correlation coefficient higher in May than in other months. For tropics, temperature consistently showed a negative correlation with GPP/SIF across all months.

In contrast to the seasonally varying temperature control of GPP/SIF, precipitation generally showed a positive correlation with GPP/SIF across all months and most regions (Fig. 5b). Radiation (SWR) overall did not show a strong control of GPP/SIF values across most months, except for negative correlations during springs across all the regions (Fig. 5c). Interestingly, the strength of SWR control of GPP/SIF was more seasonally variable in the boreal/arctic region than in other regions. And the radiation control of tropical GPP/SIF was more variable across the growing season than that of temperature or precipitation.

Furthermore, spatial analyses of the partial correlations between GPP/SIF and temperature, precipitation, and SWR confirmed the patterns on the climatic controls of GPP/SIF value revealed above (Fig. S7). Importantly, temperature control of GPP/SIF was mostly variable across different months, particularly in the temperate region; but remained largely positive and invariant in the boreal/arctic region. On the other hand, the partial correlation between SWR and GPP/SIF was variable for the boreal/arctic region but largely invariant for the temperate region. The strength of precipitation control of GPP/SIF was generally invariant across different months for most of the NH. Overall, these analyses on the correlation strength between climatic factors and GPP/SIF validated our Hypothesis H3 that changing climatic controls of GPP/SIF over time were responsible for the observed seasonality in GPP/SIF. Specifically, the varied correlation strength between temperature and GPP/SIF across different months was likely the dominant factor for GPP/SIF seasonality in the temperate region, while that between SWR and GPP/SIF was more important for GPP/SIF seasonality in the boreal/arctic region.

In light of the monthly patterns of different climatic controls of GPP/SIF variations, we visualized the seasonality (ASV) of GPP/SIF in a climatic space formed by growing season mean temperature and precipitation (Fig. 6). The strongest seasonality was found in intermediate temperature and precipitation, and decreases toward both wet and dry areas (Fig. 6). This pattern was consistent across all SIF products, especially for the intermediate temperature and precipitation ranges with the strongest GPP/SIF seasonality.

With a random forest algorithm, the climatic factors considered collectively explained over 95% of the spatial variations of GPP/SIF for all growing months. This additional analysis again confirms the highly variable climatic control of GPP/SIF across months. In Mar and Apr, pre-season solar radiation was identified as the dominant driver of the GPP/SIF variations (Fig. 7a), with GPP/SIF dropping off quickly after pre-season radiation reaches $\sim 200 \text{ W m}^{-2}$ (Fig. 7g). In May, temperature was the dominant driver of the GPP/SIF variations. GPP/SIF increased sharply when temperature increased from 0°C to 10°C , yet decreasing and then leveling off with higher temperatures (Fig. 7b).

In contrast to the early growing season when radiation and temperature dominated GPP/SIF variations, for the late growing season (June to October), precipitation, either for the present or the previous season, exerted the strongest control on the spatial variations of GPP/SIF (Fig. 7a). In all cases, GPP/SIF initially increased linearly with precipitation in water-limited areas, and then leveled off (or slightly dropped off) after reaching a certain precipitation threshold (Fig. 7a). In June and July, pre-season and current month precipitation were equally important for GPP/SIF, with thresholds of $\sim 1600 \text{ mm yr}^{-1}$ and $\sim 800 \text{ mm yr}^{-1}$ for pre-season and current precipitation, respectively (Fig. 7a, d, e). In August, pre-season precipitation was the dominant driver of GPP/SIF variations, with a precipitation threshold of $\sim 1000 \text{ mm yr}^{-1}$ (Fig. 7a, e). In September and October, present precipitation was the dominant driver of GPP/SIF variations, with a precipitation threshold of $\sim 1400 \text{ mm yr}^{-1}$ (Fig. 7a, d, e). It is also noteworthy that temperature and/or radiation could also explain considerable variations of GPP/SIF over June-October (Fig. 7a, b, f).

4. Discussion

Based on four different satellite-based SIF products, in association with FLUXCOM GPP data, we documented strong seasonal patterns of GPP/SIF across the NH. The hump-shaped GPP/SIF changes over the growing season suggest that from spring to summer, the increase of GPP is faster than that of SIF. Similarly, the decline of GPP is also faster than that of SIF moving from summer to autumn. The seasonality of GPP/SIF, measured by the difference between the maximum and minimum GPP/SIF values during March to October, showed clear geographical patterns that decreased from the boreal/arctic to temperate regions, and decreased further for drylands and tropics. We provided evidence that this seasonal pattern was also highly robust with different GPP and SIF data sets derived from a variety of satellite observations and modelling approaches, highlighting the strong seasonality of the GPP/SIF ratio. This finding of the hump-shaped GPP/SIF seasonality, together with our earlier finding of spatially-variable GPP/SIF ratios (Chen et al., 2020), suggests that the relationship between GPP and SIF should not be assumed to be constant across time or space. Thus, using a fixed SIF-GPP relationship to approximate GPP from satellite SIF observations would cause large errors in GPP magnitudes and temporal patterns. Models incorporating climatic controls, as well as their seasonal/monthly variations, on the SIF-GPP relationship would help improve the accuracy of GPP prediction from SIF (Chen et al., 2020).

Modelling algorithms have been used in the generation of these GPP and SIF products. There is a chance the seasonal pattern observed here may arise from dataset artifacts. However, considering the very different methods in deriving these gridded GPP and SIF products, for example, between FLUXCOM and MODIS GPP products, the consistency of the seasonal pattern across these different products suggest that the chance of dataset artifacts may be small. This seasonal pattern was also consistently found across different vegetation types in the mid-to-high latitudes. Wetland vegetation had a higher GPP/SIF when derived from the GOSIF product. It was noticed that SIF was slightly underestimated for this vegetation type (slope = 0.74; Li and Xiao, 2019). Since SIF values are less than 1.0, a slight, systematic underestimation of SIF could lead to an overestimation of the resulting GPP/SIF ratio.

We found that the correlation coefficient between precipitation and GPP/SIF was generally consistent across different months for both the entire Northern Hemisphere and for individual grids. On the other hand, the seasonally varying influences of temperature and radiation were likely the

primary causes for the seasonal variations in GPP/SIF in temperate and boreal/arctic regions, respectively. For temperate ecosystems, increasing temperature in spring months seemed to enhance GPP more than to stimulate SIF emission, leading to an increasing GPP/SIF ratio as temperature continues to increase from spring to summer (Fig. 5a; Fig. 7). In summer months, temperature increase has little impact on both GPP and SIF, perhaps because temperature is already at or near the optimum for photosynthesis (Huang et al., 2019). Thus, the correlation between summer temperature and GPP/SIF is close to zero or even negative. From summer to autumn, with temperature decreasing, the decline of GPP is faster than that of SIF, hence the GPP/SIF ratio declines again. By contrast, for boreal/arctic ecosystems where temperature is consistently lower than that required for optimal photosynthesis (Huang et al., 2019), warming seems to always boost photosynthetic carbon uptake more than that indicated by SIF reemission. Solar radiation, on the other hand, is consistently negatively correlated with GPP/SIF in spring months for most regions, suggesting that the increase in spring radiation stimulates more SIF reemission than photosynthetic carbon uptake when temperature is the primary factor limiting photosynthetic carbon assimilation in the cool spring. In the boreal/arctic region, however, increase radiation in summer benefits carbon assimilation and less proportion of the absorbed radiation reemits as SIF. Finally, we note that the viewing geometry may vary among different satellite products and across different months, which may also lead to seasonal variations in GPP/SIF. However, as we discussed before (Chen et al., 2020), such view geometry difference is much smaller than seasonal climatic variations (Biriukova et al., 2020). Therefore, the observed GPP/SIF variations across seasons are not likely to be primarily caused by different sensor geometries.

Mechanistic explanations for the temperature and radiation control of the seasonal variation of GPP/SIF are so far lacking. Essentially, the variation in GPP/SIF suggests that environmental and ecophysiological controls of GPP flux and SIF signals may be partly decoupled. The reason of this partial decoupling may lie in the changing allocation of incoming photons to different paths during the photosynthetic process under different climate and radiation conditions (Baker, 2008; Rosema et al., 1998; van der Tol et al., 2009). Previously, we hypothesized that changing stomatal conductance in response to water stress may explain observed spatial patterns in GPP/SIF. Here the stomatal explanation of GPP/SIF variations may still hold as precipitation consistently demonstrated a positive

correlation with GPP/SIF across all months. However, with temperature and radiation dominating the seasonal variation of GPP/SIF in the temperate and boreal/arctic regions, respectively, it seems that stomatal conductance may not be the primary cause for the seasonal pattern. Instead, we suspect that the increasing photosynthetic enzyme activity with temperature may explain the faster increase of GPP than SIF, thus increasing GPP/SIF ratios. Furthermore, as negative correlations between GPP/SIF and temperature did occur in some months, such relationships could be associated with high vapour pressure deficits (VPDs) and stomatal closure. Nonetheless, more direct evidence from field studies is needed to verify or reject the hypothesis. Furthermore, changing leaf age and leaf phenology during the growing season can strongly impact photosynthetic efficiency (Wu *et al.*, 2016; 2017) and thus may also play a role in determining the seasonal GPP/SIF variation.

In addition to these above plant physiological perspectives, canopy structure may also play some role underlying the seasonal hump-shaped GPP/SIF pattern. Satellite SIF is also affected by radiative transfer (escape ratio) while GPP is not. During the peak growing season, the canopy is denser and the escape ratio is lower compared to the early and late growing seasons. This seasonal change in canopy structure can also lead to a higher GPP/SIF ratio during the peak growing season. Since the seasonal dynamic of vegetation canopy structure (escape ratio) also has strong correlations with other climate factors, it is difficult to separate the potential contribution of canopy structure from that of climate by correlation or machine learning analyses.

Overall, our analyses revealed important seasonal patterns for the SIF-GPP relationship, which can be corroborated across several SIF products. This seasonal GPP/SIF variation highlights the importance of incorporating climate and vegetation information in the estimation of GPP from satellite SIF observations. Assuming temporal invariance of the GPP/SIF relationship to estimate GPP from SIF observations may lead to incorrect or biased conclusions about interannual and spatial variations of GPP. The underlying mechanisms for these seasonal GPP/SIF patterns require further investigation, perhaps by expanding the spatiotemporal coverage of SIF measurements in the field to encompass a broad range of phenological states, climatic conditions and vegetation types.

Acknowledgement

This work was supported in part by the Energy Exascale Earth System Model (E3SM) project, funded by the U.S. Department of Energy, Office of Science, Office of Biological and Environmental Research. A.C. and A.K.K. were supported by an Oak Ridge National Lab subcontract (4000167205).

Data Availability Statement

The GOSAT SIF data are available on request from Christian Frankenberg (cfranken@caltech.edu);

The GOME-2 SIF data are available at

https://avdc.gsfc.nasa.gov/pub/data/satellite/MetOp/GOME_F/v28/; The GOSIF data are available at

<http://globalecology.unh.edu/>; TROPOMI SIF data are available at

<ftp://fluo.gps.caltech.edu/data/tropomi/>; The FLUXCOM GPP data are available at <https://www.bgc-jena.mpg.de/geodb/projects/Data.php>; The CRU climatic data are available at <http://www.cru.uea.ac.uk/data/>.

References

Anav A, Friedlingstein P, Beer C, Ciais P, Harper A, Jones C, Murray-Tortarolo G, Papale D, Parazoo N C, Peylin P, Piao S, Sitch S, Viovy N, Wiltshire A, Zhao M. 2015. Spatiotemporal patterns of terrestrial gross primary production: A review. *Reviews of Geophysics*, 53 (3): 785-818

Baker N R. 2008. Chlorophyll Fluorescence: A Probe of Photosynthesis In Vivo. *Annual Review of Plant Biology*, 59 (1): 89-113

Beer C, Reichstein M, Tomelleri E, Ciais P, Jung M, Carvalhais N, Rödenbeck C, Arain M A, Baldocchi D, Bonan G B, Bondeau A, Cescatti A, Lasslop G, Lindroth A, Lomas M, Luyssaert S, Margolis H, Oleson K W, Roupsard O, Veenendaal E, Viovy N, Williams C, Woodward F I, Papale D. 2010. Terrestrial Gross Carbon Dioxide Uptake: Global Distribution and Covariation with Climate. *Science*, 329 (5993): 834-838

Buermann, W., Forkel, M., O'Sullivan, M., Sitch, S., Friedlingstein, P., Haverd, V., Jain, A.K., Kato, E., Kautz, M., Lienert, S., Lombardozzi, D.A., Nabel, J.E.M.S., Tian, H.Q., Wiltshire, A.J., Zhu,

D., Smith, W.K., Richardson, A.D. (2018) Widespread seasonal compensation effects of spring warming on northern plant productivity. *Nature* 562, 110-+.

Chen, A., Mao, J., Ricciuto, D., Xiao, J., Frankenberg, C., Li, X., Thornton, P.E., Gu, L. and Knapp, A.K., 2020. Moisture availability mediates the relationship between terrestrial gross primary production and solar-induced fluorescence: Insights from global scale variations. *Global Change Biology*.

Frankenberg C, Fisher J B, Worden J, Badgley G, Saatchi S S, Lee J-E, Toon G C, Butz A, Jung M, Kuze A, Yokota T. 2011. New global observations of the terrestrial carbon cycle from GOSAT: Patterns of plant fluorescence with gross primary productivity. *Geophysical Research Letters*, 38 (17):

Fu, Y.H., Piao, S., Zhao, H., Jeong, S.-J., Wang, X., Vitasse, Y., Ciais, P., Janssens, I.A. (2014) Unexpected role of winter precipitation in determining heat requirement for spring vegetation green-up at northern middle and high latitudes. *Global Change Biology*, 20, 3743-3755.

Fu, Y.H., Zhao, H., Piao, S., Peaucelle, M., Peng, S., Zhou, G., Ciais, P., Huang, M., Menzel, A., Penuelas, J., Song, Y., Vitasse, Y., Zeng, Z., Janssens, I.A. (2015) Declining global warming effects on the phenology of spring leaf unfolding. *Nature* 526, 104-107.

Gu L, Han J, Wood J D, Chang C Y-Y, Sun Y. 2019. Sun-induced Chl fluorescence and its importance for biophysical modeling of photosynthesis based on light reactions. *New Phytologist*, 223 (3): 1179-1191

Guanter L, Frankenberg C, Dudhia A, Lewis P E, Gómez-Dans J, Kuze A, Suto H, Grainger R G. 2012. Retrieval and global assessment of terrestrial chlorophyll fluorescence from GOSAT space measurements. *Remote Sensing of Environment*, 121: 236-251

Guanter L, Zhang Y, Jung M, Joiner J, Voigt M, Berry J A, Frankenberg C, Huete A R, Zarco-Tejada P, Lee J-E, Moran M S, Ponce-Campos G, Beer C, Camps-Valls G, Buchmann N, Gianelle D, Klumpp K, Cescatti A, Baker J M, Griffis T J. 2014. Global and time-resolved monitoring of crop photosynthesis with chlorophyll fluorescence. *Proceedings of the National Academy of Sciences*, 111 (14): E1327-E1333

He M, Ju W, Zhou Y, Chen J, He H, Wang S, Wang H, Guan D, Yan J, Li Y, Hao Y, Zhao F. 2013. Development of a two-leaf light use efficiency model for improving the calculation of terrestrial gross primary productivity. *Agricultural and Forest Meteorology*, 173: 28-39

Hilker T, Coops N C, Wulder M A, Black T A, Guy R D. 2008. The use of remote sensing in light use efficiency based models of gross primary production: A review of current status and future requirements. *Science of the Total Environment*, 404 (2): 411-423

Jeong, S. J., Schimel, D., Frankenberg, C., Drewry, D. T., Fisher, J. B., Verma, M., Berry, J. A., Lee, J. E., & Joiner, J. (2017). Application of satellite solar-induced chlorophyll fluorescence to understanding large-scale variations in vegetation phenology and function over northern high latitude forests. *Remote Sensing of Environment*, 190, 178– 187.

Joiner J, Yoshida Y, Vasilkov A P, Yoshida Y, Corp L A, Middleton E M. 2011. First observations of global and seasonal terrestrial chlorophyll fluorescence from space. *Biogeosciences*, 8 (3): 637-651

Keenan T F, Davidson E, Moffat A M, Munger W, Richardson A D. 2012. Using model-data fusion to interpret past trends, and quantify uncertainties in future projections, of terrestrial ecosystem carbon cycling. *Global Change Biology*, 18 (8): 2555-2569

Li X, Xiao J, He B, Altaf Arain M, Beringer J, Desai A R, Emmel C, Hollinger D Y, Krasnova A, Mammarella I, Noe S M, Ortiz P S, Rey-Sanchez A C, Rocha A V, Varlagin A. 2018. Solar-induced chlorophyll fluorescence is strongly correlated with terrestrial photosynthesis for a wide variety of biomes: First global analysis based on OCO-2 and flux tower observations. *Global Change Biology*, 24 (9): 3990-4008

Magney T S, Bowling D R, Logan B A, Grossmann K, Stutz J, Blanken P D, Burns S P, Cheng R, Garcia M A, Köhler P, Lopez S, Parazoo N C, Racza B, Schimel D, Frankenberg C. 2019. Mechanistic evidence for tracking the seasonality of photosynthesis with solar-induced fluorescence. *Proceedings of the National Academy of Sciences*, 116 (24): 11640-11645

Meroni M, Rossini M, Guanter L, Alonso L, Rascher U, Colombo R, Moreno J. 2009. Remote sensing of solar-induced chlorophyll fluorescence: Review of methods and applications. *Remote Sensing of Environment*, 113 (10): 2037-2051

Mohammed G H, Colombo R, Middleton E M, Rascher U, Van Der Tol C, Nedbal L, Goulas Y, Pérez-Priego O, Damm A, Meroni M, Joiner J, Cogliati S, Verhoef W, Malenovský Z, Gastellu-Etchegorry J-P, Miller J R, Guanter L, Moreno J, Moya I, Berry J A, Frankenberg C, Zarco-Tejada P J. 2019. Remote sensing of solar-induced chlorophyll fluorescence (SIF) in vegetation: 50 years of progress. *Remote Sensing of Environment*, 231: 111177

Parazoo N C, Bowman K, Fisher J B, Frankenberg C, Jones D B A, Cescatti A, Pérez-Priego Ó, Wohlfahrt G, Montagnani L. 2014. Terrestrial gross primary production inferred from satellite fluorescence and vegetation models. *Global Change Biology*, 20 (10): 3103-3121

Porcar-Castell A, Tyystjärvi E, Atherton J, Van Der Tol C, Flexas J, Pfundel E E, Moreno J, Frankenberg C, Berry J A. 2014. Linking chlorophyll a fluorescence to photosynthesis for remote sensing applications: mechanisms and challenges. *Journal of Experimental Botany*, 65 (15): 4065-4095

Prince S D, Goward S N. 1995. Global Primary Production: A Remote Sensing Approach. *Journal of biogeography*, 22 (4/5): 815-835

Rosema A, Snel J F H, Zahn H, Buurmeijer W F, Van Hove L W A. 1998. The Relation between Laser-Induced Chlorophyll Fluorescence and Photosynthesis. *Remote Sensing of Environment*, 65 (2): 143-154

Running S W, Nemani R R, Heinsch F A, Zhao M, Reeves M, Hashimoto H. 2004. A Continuous Satellite-Derived Measure of Global Terrestrial Primary Production. *Bioscience*, 54 (6): 547-560

Sitch S, Huntingford C, Gedney N, Levy P E, Lomas M, Piao S L, Betts R, Ciais P, Cox P, Friedlingstein P, Jones C D, Prentice I C, Woodward F I. 2008. Evaluation of the terrestrial carbon cycle, future plant geography and climate-carbon cycle feedbacks using five Dynamic Global Vegetation Models (DGVMs). *Global Change Biology*, 14 (9): 2015-2039

Sjöström M, Zhao M, Archibald S, Arneth A, Cappelaere B, Falk U, De Grandcourt A, Hanan N, Kergoat L, Kutsch W, Merbold L, Mougin E, Nickless A, Nouvellon Y, Scholes R J, Veenendaal E M, Ardö J. 2013. Evaluation of MODIS gross primary productivity for Africa using eddy covariance data. *Remote Sensing of Environment*, 131: 275-286

Sun Y, Frankenberg C, Wood J D, Schimel D S, Jung M, Guanter L, Drewry D T, Verma M, Porcar-Castell A, Griffis T J, Gu L, Magney T S, Köhler P, Evans B, Yuen K. 2017. OCO-2 advances photosynthesis observation from space via solar-induced chlorophyll fluorescence. *Science*, 358 (6360): eaam5747

Tan, J., Piao, S., Chen, A., Zeng, Z., Ciais, P., Janssens, I. A., ... & Vicca, S. 2015. Seasonally different response of photosynthetic activity to daytime and night-time warming in the Northern Hemisphere. *Global change biology*, 21(1): 377-387

Tucker C J, Fung I Y, Keeling C D, Gammon R H. 1986. Relationship between atmospheric CO₂ variations and a satellite-derived vegetation index. *Nature*, 319 (6050): 195-199

Turner D P, Ritts W D, Cohen W B, Gower S T, Zhao M, Running S W, Wofsy S C, Urbanski S, Dunn A L, Munger J W. 2003. Scaling Gross Primary Production (GPP) over boreal and deciduous forest landscapes in support of MODIS GPP product validation. *Remote Sensing of Environment*, 88 (3): 256-270

Turner D P, Ritts W D, Cohen W B, Gower S T, Running S W, Zhao M, Costa M H, Kirschbaum A A, Ham J M, Saleska S R, Ahl D E. 2006. Evaluation of MODIS NPP and GPP products across multiple biomes. *Remote Sensing of Environment*, 102 (3): 282-292

Van Der Tol C, Verhoef W, Rosema A. 2009. A model for chlorophyll fluorescence and photosynthesis at leaf scale. *Agricultural and Forest Meteorology*, 149 (1): 96-105

Wen J, Köhler P, Duveiller G, Parazoo N C, Magney T S, Hooker G, Yu L, Chang C Y, Sun Y. 2020. A framework for harmonizing multiple satellite instruments to generate a long-term global high spatial-resolution solar-induced chlorophyll fluorescence (SIF). *Remote Sensing of Environment*, 239: 111644

Wu J, Serbin S P, Xu X, Albert L P, Chen M, Meng R, Saleska S R, Rogers A. 2017. The phenology of leaf quality and its within-canopy variation is essential for accurate modeling of photosynthesis in tropical evergreen forests. *Global Change Biology*, 23 (11): 4814-4827

Xiao J, Zhuang Q, Law B E, Chen J, Baldocchi D D, Cook D R, Oren R, Richardson A D, Wharton S, Ma S, Martin T A, Verma S B, Suyker A E, Scott R L, Monson R K, Litvak M, Hollinger D Y, Sun G, Davis K J, Bolstad P V, Burns S P, Curtis P S, Drake B G, Falk M, Fischer M L, Foster D R, Gu L, Hadley J L, Katul G G, Matamala R, McNulty S, Meyers T P, Munger J W,

Noormets A, Oechel W C, Paw U K T, Schmid H P, Starr G, Torn M S, Wofsy S C. 2010. A continuous measure of gross primary production for the conterminous United States derived from MODIS and AmeriFlux data. *Remote Sensing of Environment*, 114 (3): 576-591

Xiao J, Li X, He B, Arain M A, Beringer J, Desai A R, Emmel C, Hollinger D Y, Krasnova A, Mammarella I, Noe S M, Serrano Ortiz P, Rey-Sanchez C, Rocha A V, Varlagin A. 2019. Solar-induced chlorophyll fluorescence exhibits a universal relationship with gross primary productivity across a wide variety of biomes. *Global Change Biology*, 25 (4): e4-e6

Xu C, Liu H, Williams A P, Yin Y, Wu X. 2016. Trends toward an earlier peak of the growing season in Northern Hemisphere mid-latitudes. *Global Change Biology*, 22 (8): 2852-2860

Yang H, Yang X, Zhang Y, Heskell M A, Lu X, Munger J W, Sun S, Tang J. 2017. Chlorophyll fluorescence tracks seasonal variations of photosynthesis from leaf to canopy in a temperate forest. *Global Change Biology*, 23 (7): 2874-2886

Yuan W, Liu S, Yu G, Bonnefond J-M, Chen J, Davis K, Desai A R, Goldstein A H, Gianelle D, Rossi F, Suyker A E, Verma S B. 2010. Global estimates of evapotranspiration and gross primary production based on MODIS and global meteorology data. *Remote Sensing of Environment*, 114 (7): 1416-1431

Zhang Y, Guanter L, Berry J A, Van Der Tol C, Yang X, Tang J, Zhang F. 2016. Model-based analysis of the relationship between sun-induced chlorophyll fluorescence and gross primary production for remote sensing applications. *Remote Sensing of Environment*, 187: 145-155

Zhang, Yao, Xiao, X., Zhang, Yongguang, Wolf, S., Zhou, S., Joiner, J., Guanter, L., Verma, M., Sun, Y., Yang, X., Paul-Limoges, E., Gough, C.M., Wohlfahrt, G., Gioli, B., van der Tol, C., Yann, N., Lund, M., de Grandcourt, A., 2018. On the relationship between sub-daily instantaneous and daily total gross primary production: Implications for interpreting satellite-based SIF retrievals. *Remote Sensing of Environment* 205, 276–289. <https://doi.org/10.1016/j.rse.2017.12.009>

Zhang Z, Zhang Y, Joiner J, Migliavacca M. 2018. Angle matters: Bidirectional effects impact the slope of relationship between gross primary productivity and sun-induced chlorophyll fluorescence from Orbiting Carbon Observatory-2 across biomes. *Global Change Biology*, 24 (11): 5017-5020

Accepted Article

This article is protected by copyright. All rights reserved

Figure Legends

Fig. 1. Average monthly GPP/SIF (\pm SD range) for different regions over the Northern Hemisphere (NH) during the growing season. Please note that GPP and SIF values have been normalized to [0,1] before calculating their ratios. The definition of the growing season length for each grid followed Zhu et al. (2016). For each region, we only included months with 50% or more of its area in the growing season. Each subfigure was derived from FLUXCOM GPP and one of the following SIF products: (a) GOME-2, (b) GOSAT, (c) GOSIF, and (d) TROPOMI. GPP, gross primary production; SIF, solar-induced chlorophyll fluorescence.

Fig. 2. Average monthly GPP/SIF (\pm SD range) for different vegetation types over the Northern Hemisphere (NH) during the growing season. The definition of the growing season length for each grid followed Zhu et al. (2016). For each vegetation type, we only included months when 50% or more of the area of that vegetation type falls within the growing season. Each subfigure was derived from FLUXCOM GPP and one of the following SIF products: (a, e) GOME-2, (b, f) GOSAT, (c, g) GOSIF, and (d, h) TROPOMI.

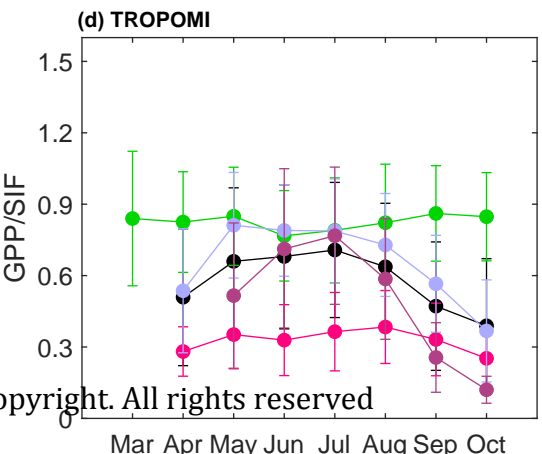
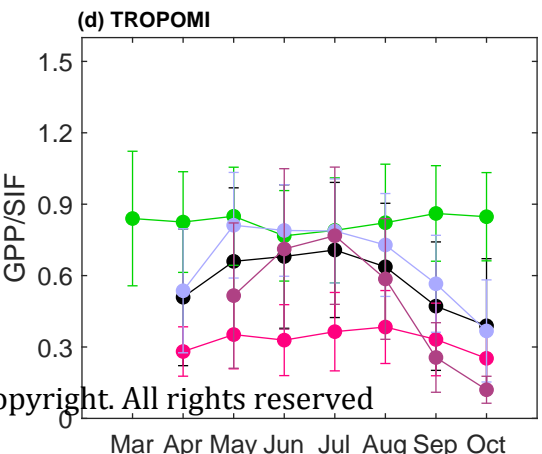
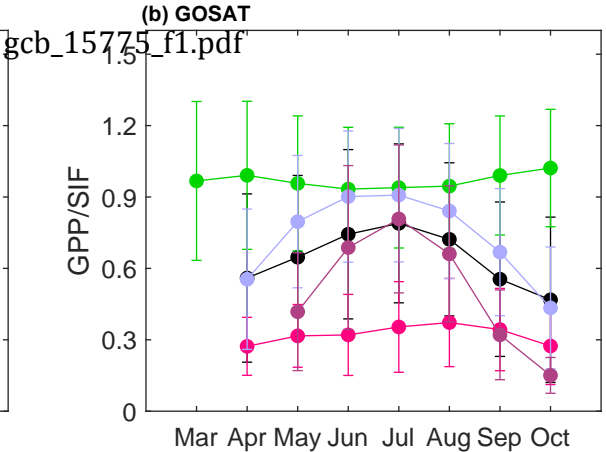
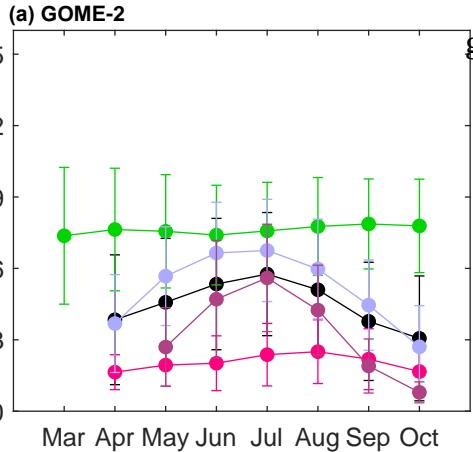
Fig. 3. The spatial distribution of the amplitude of seasonal variation (ASV) in GPP/SIF. Here ASV was calculated as the difference between highest and lowest monthly GPP/SIF values during the growing season. The definition of the growing season length for each grid followed Zhu et al. (2016). Each subfigure was derived from FLUXCOM GPP and one of the following SIF products: (a) GOME-2, (b) GOSAT, (c) GOSIF, and (d) TROPOMI.

Fig. 4. The spatial distribution of the month with the (a) minimum and (b) maximum GPP/SIF values. The pie figure in the insets shows the percentage of different months for all the grids.

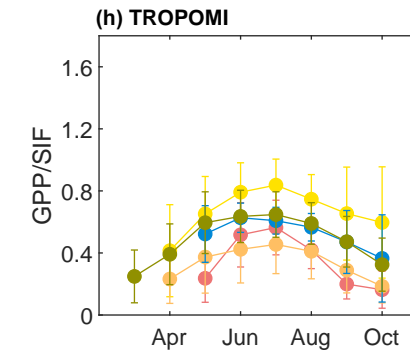
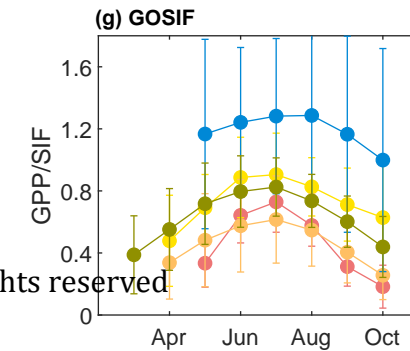
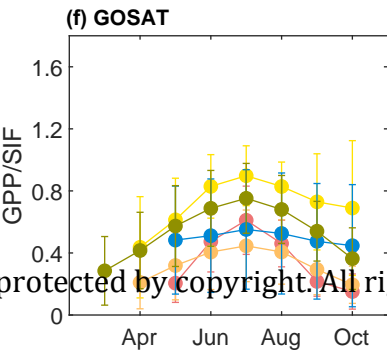
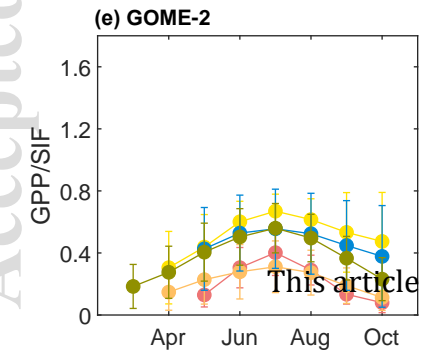
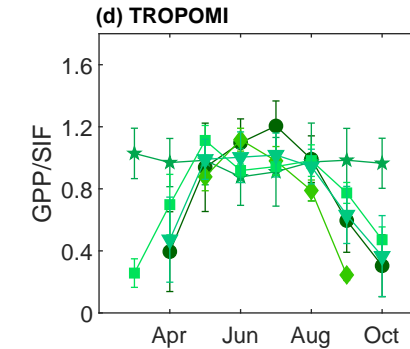
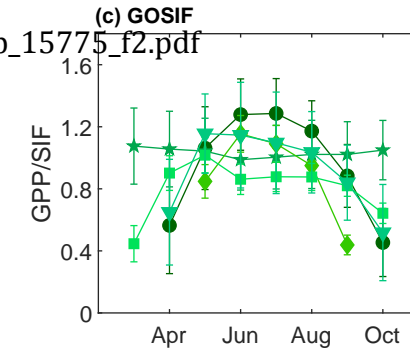
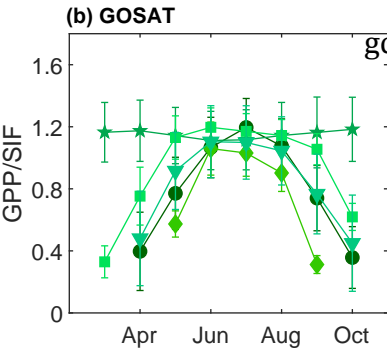
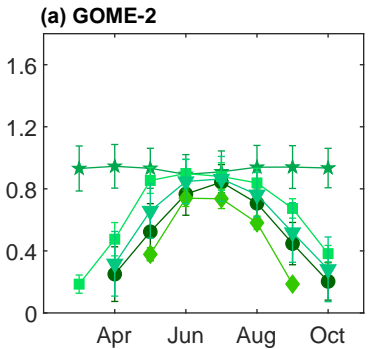
Fig. 5. Box-whisker plot of the distribution of partial correlation between monthly GPP/SIF and climate variables: (a) temperature, (b) precipitation, and (c) short wave radiation, over the Northern Hemisphere (NH) and for different regions during the growing season.

Fig. 6. The distribution of the seasonal amplitude (ASV) in GPP/SIF across the temperature-precipitation space. Note that both GPP and SIF were normalized before calculating GPP/SIF ratios. ASV was calculated as the difference between highest and lowest monthly GPP/SIF during March to October. Each climatic bin is 4°C (temperature) by 1mm day^{-1} (precipitation).

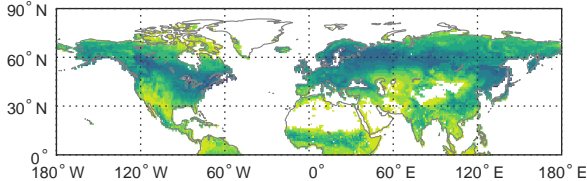
Fig. 7. Relationship between the GPP/SIF ratio and climatic factors based on a random forest algorithm. (a), the importance rank of climatic factors to the spatial variations of the monthly GPP/SIF ratio. (b-g), the partial dependence of the GPP/SIF ratio on present-season temperature (b), pre-season (PS) temperature (c), present-season precipitation (d), PS precipitation (e), present-season shortwave radiation (f) and PS shortwave radiation (g).



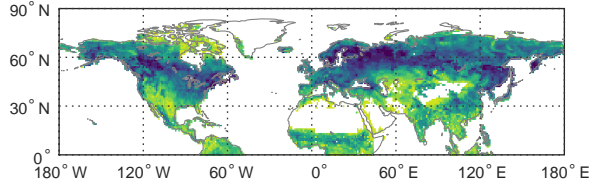
This article is protected by copyright. All rights reserved



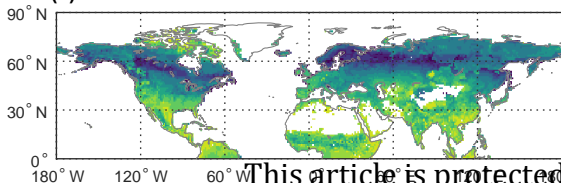
(a) GOME-2



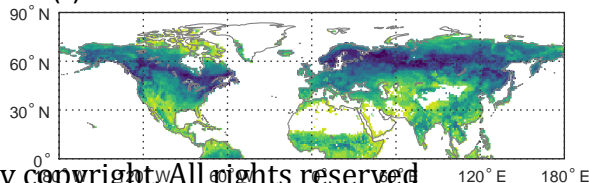
(b) GOSAT



(c) GOSIF



(d) TROPOMI

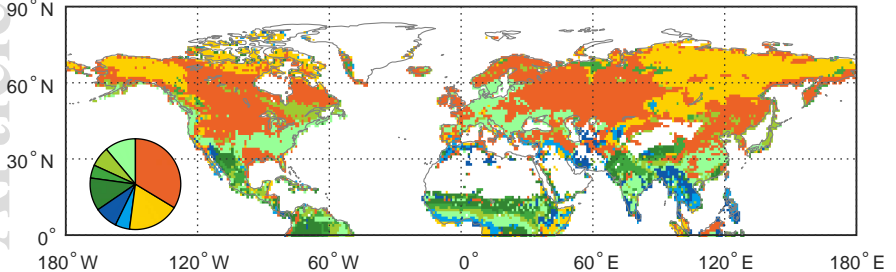


This article is protected by copyright. All rights reserved

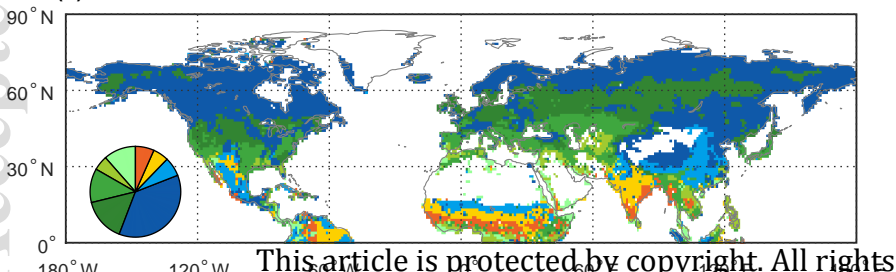


(a) Minimum

gcb_15775_f4.pdf

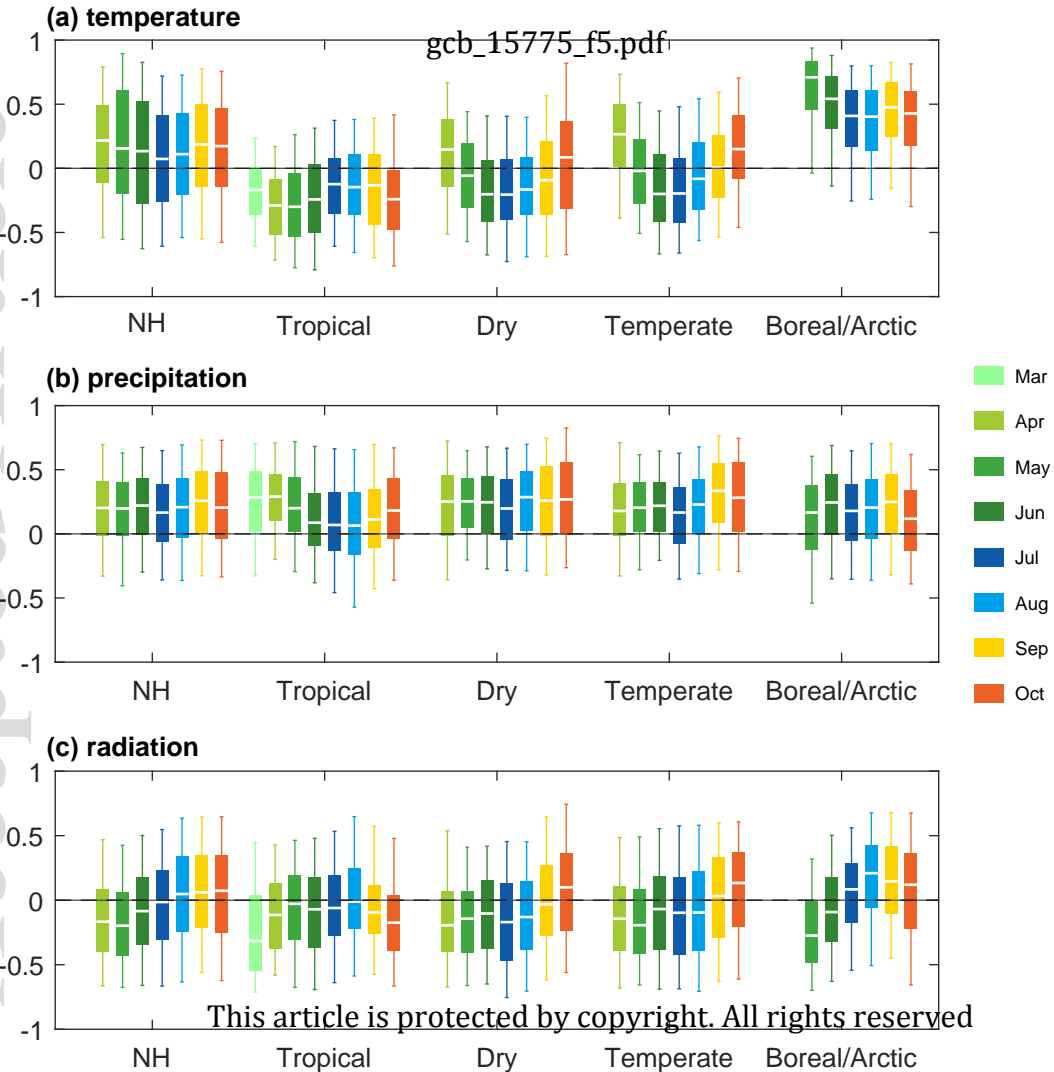


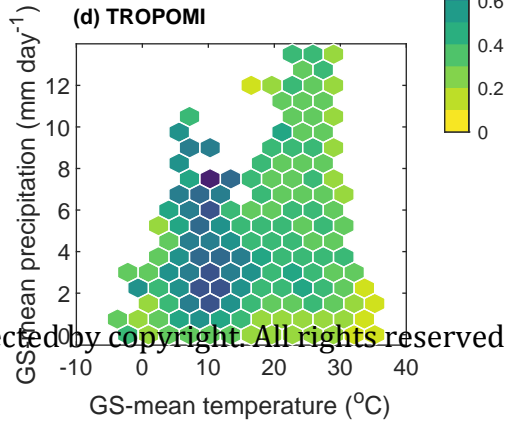
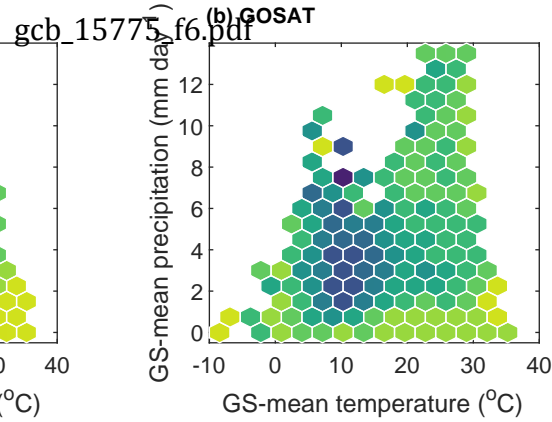
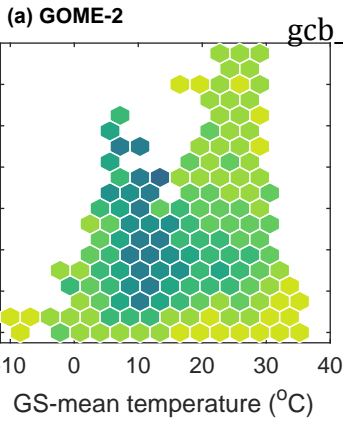
(b) Maximum



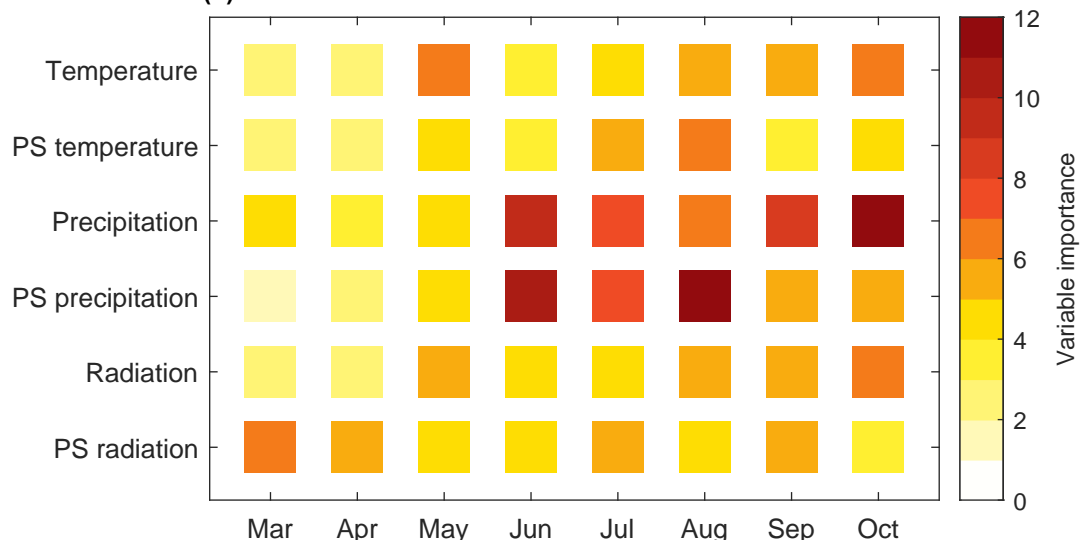
This article is protected by copyright. All rights



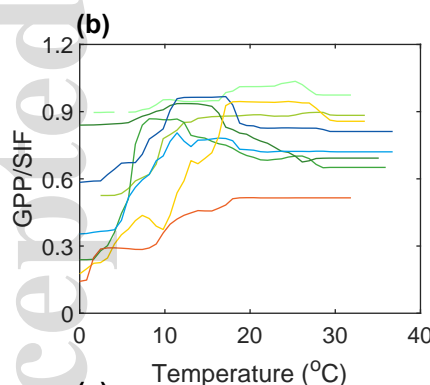




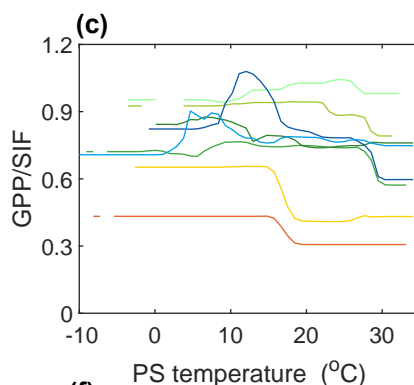
(a)



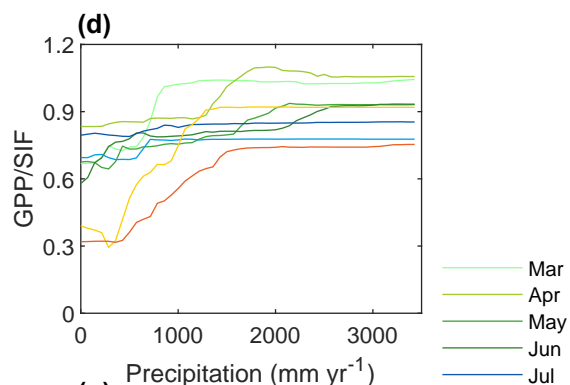
(b)



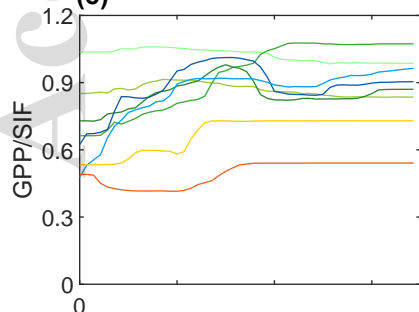
(c)



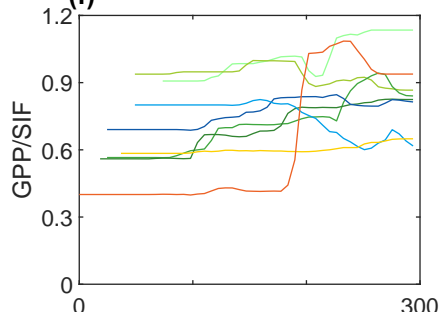
(d)



(e)



(f)



(g)

